ARTICLE

BIOTECHNOLOGY and BIOENGINEERING

Genome-Scale Analysis of *Saccharomyces cerevisiae* Metabolism and Ethanol Production in Fed-Batch Culture

Jared L. Hjersted,[1] Michael A. Henson,[1] Radhakrishnan Mahadevan[2]

[1]Department of Chemical Engineering, University of Massachusetts,
159 Goessmann Laboratory, 686 North Pleasant Street, Amherst, Massachusetts 01003-3110;
telephone: 413-545-3481; fax: 413-545-1647; e-mail: henson@ecs.umass.edu

[2]Department of Chemical Engineering and Applied Chemistry, University of Toronto,
Toronto, Ontario M5S 3E5, Canada

Received 17 August 2006; accepted 28 December 2006

Published online 22 January 2007 in Wiley InterScience (www.interscience.wiley.com). DOI 10.1002/bit.21332

ABSTRACT: A dynamic flux balance model based on a genome-scale metabolic network reconstruction is developed for in silico analysis of *Saccharomyces cerevisiae* metabolism and ethanol production in fed-batch culture. Metabolic engineering strategies previously identified for their enhanced steady-state biomass and/or ethanol yields are evaluated for fed-batch performance in glucose and glucose/xylose media. Dynamic analysis is shown to provide a single quantitative measure of fed-batch ethanol productivity that explicitly handles the possible tradeoff between the biomass and ethanol yields. Productivity optimization conducted to rank achievable fed-batch performance demonstrates that the genetic manipulation strategy and the fed-batch operating policy should be considered simultaneously. A library of candidate gene insertions is assembled and directly screened for their achievable ethanol productivity in fed-batch culture. A number of novel gene insertions with ethanol productivities identical to the best metabolic engineering strategies reported in previous studies are identified, thereby providing additional targets for experimental evaluation. The top performing gene insertions were substrate dependent, with the highest ranked insertions for glucose media yielding suboptimal performance in glucose/xylose media. The analysis results suggest that enhancements in biomass yield are most beneficial for the enhancement of fed-batch ethanol productivity by recombinant xylose utilizing yeast strains. We conclude that steady-state flux balance analysis is not sufficient to predict fed-batch performance and that the media, genetic manipulations, and fed-batch operating policy should be considered simultaneously to achieve optimal metabolite productivity.

Biotechnol. Bioeng. 2007;97: 1190–1204.

KEYWORDS: *Saccharomyces cerevisiae*; dynamic flux balance analysis; genome-scale metabolic network; fed-batch culture; metabolic engineering

Introduction

The availability of genome-scale stoichiometric models of cellular metabolism (Reed et al., 2006) has enabled the development of computational algorithms for the analysis and design of complex metabolic networks. A popular approach is flux balance analysis (FBA), where a linear programming problem is posed to resolve the intracellular fluxes in an underdetermined stoichiometric model under the assumption that the cell utilizes available resources for growth rate maximization (Stephanopoulos et al., 1998). FBA has been used extensively for predicting cellular growth and product secretion patterns in microbial systems (Kauffman et al., 2003; Sauer et al., 1996; Segre et al., 2002). Extensions of classical FBA allow the redesign of metabolic networks for the overproduction of desired metabolites through gene deletions and insertions, which are implemented by removing or adding intracellular reactions to the network. These computational methods provide metabolic engineering targets that are experimentally testable. In a recent study with a *Saccharomyces cerevisiae* genome-scale network, the growth phenotypes of gene knockouts were predicted with a ≈70–80% success rate (Famili et al., 2003). Several computational studies of gene manipulations for metabolite overproduction have been presented (Bro et al., 2006; Burgard and Maranas, 2001; Pharkya et al., 2004).

These FBA methods assume time-invariant extracellular conditions and generate steady-state predictions consistent with continuous culture. However, large-scale production of metabolic products is often achieved with batch and

Correspondence to: M.A. Henson

fed-batch culture. An important advantage of fed-batch culture is that substrate levels can be transiently varied to achieve a favorable tradeoff between cellular growth and product formation rates. Although batch culture experiments are often used to evaluate FBA predictions, the results are strictly valid only for the balanced growth phase. An alternative is to perform metabolic network analysis and design using dynamic extensions of stoichiometric models. Dynamic flux balance models are obtained by combining stoichiometric equations for intracellular metabolism with dynamic mass balances on key extracellular substrates and products under the assumption of fast intracellular dynamics (Gadkar et al., 2004; Hjersted and Henson, 2006; Mahadevan et al., 2002; Sainz et al., 2003; Varma and Palsson, 1994). The intracellular and extracellular descriptions are coupled through the cellular growth rate and substrate uptake kinetics, which can be formulated to include key regulatory effects such as product inhibition of growth. Batch culture simulations with dynamic flux balance models have shown good agreement with experimental data (Sainz et al., 2003; Varma and Palsson, 1994).

Dynamic flux balance modeling offers important advantages over alternative dynamic modeling frameworks. Because simple unstructured models rely on phenomenological descriptions of cell growth and constant yield coefficients (Nielsen and Villadsen, 1994), they have no predictive capability for genetic alterations. Metabolic engineering applications of structured kinetic models (Steinmeyer and Shuler, 1989; Vaseghi et al., 1999), log-linear kinetic models (Hatzimanikatis et al., 1998), and cybernetic models (Jones and Kompala, 1999; Varner and Ramkrishna, 1999) are often limited by the lack of parameter values for in vivo enzyme kinetics. Dynamic flux balance modeling provides a practical alternative for incorporating intracellular structure. Given the availability of a steady-state flux balance model, only a small number of additional parameters are needed to account for the uptake of multiple substrates and the secretion of multiple products. On the other hand, a well documented weakness of classical FBA is the difficulty associated with incorporating cellular regulation. This problem has been partially addressed by using gene expression data to constrain regulated fluxes within the metabolic network (Åkesson et al., 2004; Covert et al., 2001). Dynamic flux balance analysis (DFBA) offers the additional possibility of formulating substrate uptake kinetics to account for known regulatory processes.

The production of ethanol from recombinant yeast strains has received considerable attention for renewable liquid fuel applications. Of particular interest is genetic engineering of xylose fermenting strains that can grow on media derived from agricultural products such as corn (Aristidou and Penttila, 2000; Jeffries and Jin, 2004; Kuyper et al., 2005; Ostergaard et al., 2000). A recent study by Bro et al. (2006) revealed novel metabolic engineering targets for improved ethanol production from glucose media based on classical FBA of a genome-scale *S. cerevisiae* metabolic network. One of the most promising strategies was shown experimentally to outperform wild-type *S. cerevisiae* in both glucose and glucose/xylose media. In addition to being limited to steady-state culture conditions, this computational analysis failed to explicitly address the well-known tradeoff between the biomass and ethanol yields. Moreover, regulatory processes such as ethanol inhibition of growth that are active under dynamic culture conditions might lead to favorable metabolic engineering strategies that are not easily identifiable from steady-state analysis.

The computational study reported in this paper focuses on genome-scale analysis of a *S. cerevisiae* dynamic flux balance model to analyze existing and uncover new metabolic engineering strategies for ethanol overproduction from glucose and glucose/xylose media in fed-batch culture. A fully compartmentalized and charge balanced network reconstruction (Duarte et al., 2004) is combined with extracellular mass balance on growth substrates (glucose, xylose, oxygen) and competing metabolic products (ethanol, glycerol, xylitol). To our knowledge, the developed model represents the first attempt to incorporate a genome-scale metabolic reconstruction into the dynamic flux balance framework. Dynamic analysis of ten metabolic engineering strategies reported in the steady-state FBA study of Bro et al. (2006) are evaluated with respect to their achievable ethanol productivities in fed-batch culture. A library of candidate gene insertions is dynamically screened to identify new metabolic engineering targets for enhanced fed-batch ethanol productivity.

Methods

Dynamic Flux Balance Model

A fed-batch model for aerobic and anaerobic growth of *S. cerevisiae* on glucose and xylose media was developed. The model consisted of intracellular steady-state flux balances coupled to dynamic extracellular mass balances through kinetic uptake expressions for three possible substrates (glucose, xylose, oxygen). The *S. cerevisiae* genome-scale metabolic network model *i*ND750 was used in this study (Duarte et al., 2004; http://gcrg.ucsd.edu/organisms/yeast.html). Each reaction is fully charged balanced and elementally mass balanced with respect to carbon and hydrogen. The model is fully compartmentalized with 750 genes and 1,149 intracellular reactions, which are divided into the cytosol, mitochondrion, peroxisome, nucleus, endoplasmic reticulum, Golgi apparatus, and vacuole. Compartmentalization of the 646 unique metabolites produces 1,059 species that are stoichiometrically balanced. The dimensions of the stoichiometric matrix for the *i*ND750 model are 1,059 species and 1,264 fluxes, which includes the intracellular reactions and 115 membrane exchange fluxes. The publicly available model includes a mostly complete description of xylose metabolism such that the associated pathways become active only when a xylose

uptake rate is specified. The only modification needed for simulation of recombinant xylose utilizing strains was the insertion of the reverse reaction for xylitol dehydrogenase, which increased the number of fluxes to 1,265 for mixed-substrate studies.

The linear program (LP) to resolve the underdetermined flux balances was formulated as:

$$\begin{aligned} \max_{v} \quad & \mu = \sum_{j} w_j v_j \\ \text{subject to :} \quad & Av = 0 \\ & v_{\min} \le v \le v_{\max} \end{aligned} \tag{1}$$

where A is the stoichiometric matrix for the metabolic network, v is a vector of reaction and exchange fluxes, and $v_{\max}$ and $v_{\min}$ are vectors for upper and lower flux bounds, respectively. The cellular growth rate (μ) was calculated from the fluxes producing biomass precursors where the weights (w) were determined from the amount of each precursor necessary for biomass formation (Duarte et al., 2004). We did not constrain the metabolic network to account for known differences between the aerobic and anaerobic metabolism of *S. cerevisiae* (Åkesson et al., 2004) due to the difficulty associated with incorporating steady-state gene expression data into our dynamic model. Despite this omission, we were able to generate dynamic predictions consistent with experimental data over a wide range of aerobic and anaerobic conditions.

The uptake kinetics for glucose (v_g), xylose (v_z), and oxygen (v_o) were modeled as:

$$v_g = v_{g,\max} \frac{G}{K_g + G} \frac{1}{1 + \frac{E}{K_{ie}}} \tag{2}$$

$$v_z = v_{z,\max} \frac{Z}{K_z + Z} \frac{1}{1 + \frac{E}{K_{ie}}} \frac{1}{1 + \frac{G}{K_{ig}}} \tag{3}$$

$$v_o = v_{o,\max} \frac{O}{K_o + O} \tag{4}$$

where G, Z, E, and O are the glucose, xylose, ethanol, and dissolved oxygen concentrations, respectively, K_g, K_z, and K_o are saturation constants, $v_{g,\max}$, $v_{z,\max}$, and $v_{o,\max}$ are maximum uptake rates, and K_{ie} and K_{ig} are inhibition constants. The glucose uptake followed Michaelis–Menten kinetics with an additional regulatory term to capture growth rate suppression due to high ethanol concentrations (Sainz et al., 2003). The xylose uptake had a similar form with an additional regulatory term to account for inhibited xylose metabolism in the presence of the preferred substrate glucose (Kuyper et al., 2005). Ethanol uptake was excluded from the model because ethanol consumption is oxidative and only experimentally observed when glucose is nearly exhausted (Jones and Kompala, 1999), conditions which do not occur in the simulations considered in this study.

The dynamic mass balances on the extracellular environment were posed as:

$$\frac{dV}{dt} = F \tag{5}$$

$$\frac{d(VX)}{dt} = \mu VX \tag{6}$$

$$\frac{d(VG)}{dt} = FG_f - v_g VX \tag{7}$$

$$\frac{d(VZ)}{dt} = FZ_f - v_z VX \tag{8}$$

$$\frac{d(VE)}{dt} = v_e VX \tag{9}$$

where V is the liquid volume, X is the biomass concentration, G_f and Z_f are the glucose and xylose feed concentrations, respectively, and F is the feed flow rate. The growth rate (μ) and the ethanol exchange flux (v_e) were resolved by solution of the inner flux balance model. Although not shown here, analogous equations were posed for key metabolic byproducts (glycerol and xylitol). The dissolved oxygen concentration was treated as an input variable under the assumption that its dynamic profile could be tracked by a suitably designed feedback controller. This simplification was deemed reasonable because anaerobic conditions were used to promote ethanol production during later stages of the batch when high cell densities that might limit oxygen mass transfer were encountered. Consequently, extracellular oxygen balances were omitted and the dissolved oxygen concentration was simply represented as the percent of saturation: $DO = O/O_{sat}$ where O_{sat} is the saturation concentration.

Metabolic Engineering Strategies

Genetic manipulations involving gene deletions, gene overexpressions, and gene insertions for ethanol overproduction were considered in this study. Steady-state FBA and DFBA were applied to eleven previously suggested metabolic engineering strategies. These strategies included eight gene insertions and two combination gene insertion/overexpression strategies that were predicted to enhance biomass and/or ethanol yields when classical FBA was applied to the *i*FF708 *S. cerevisiae* metabolic network model (Bro et al., 2006). We performed the same steady-state analysis on the *i*ND750 model, which represents a second generation improvement of the *i*FF708 reconstruction, to provide a consistent basis for comparing our DFBA results. The ten strategies were implemented by the addition of reactions to the metabolic network for gene insertions, by the removal of reactions for gene deletions, and by the removal of bound constraints from reactions for gene

DOI 10.1002/bit

overexpressions as discussed by Bro et al. (2006). An additional gene deletion strategy was considered. The *aac1* gene is associated with oxidative phosphorylation, and the knockout Δ*aac1* has been shown to be experimentally viable (Giaever et al., 2002; Lawson et al., 1990). While this knockout has no effect under anaerobic conditions, our preliminary analysis showed that higher ethanol yields at the expense of reduced biomass yields were predicted for aerobic conditions. We performed analysis of the Δ*aac1* knockout to examine the tradeoff between these two competing factors in fed-batch culture, where an initial aerobic phase used to produce biomass is followed by an anaerobic phase that promotes ethanol formation (Hjersted and Henson, 2006).

We also assembled a library of 357 gene insertion candidates from the LIGAND database in the Kyoto Encyclopedia of Genes and Genomes (KEGG) (Kanehisa, 1997; Kanehisa and Goto, 2000; Kanehisa et al., 2006) (http://www.genome.jp/) in an attempt to uncover novel metabolic engineering strategies for ethanol overproduction in fed-batch culture. Only reactions involving species present in the cytosol of *i*ND750 were considered for this study. We were able to match 517 of the 575 cytosolic species in *i*ND750 to compounds in the LIGAND database, and 788 reactions involved only these matched species. The *i*ND750 metabolic network already included 431 of these reactions, yielding a reduced set of 357 reactions corresponding to potential gene insertions. All reactions were assumed reversible unless available experimental data suggested otherwise.

Because the *i*ND750 model is fully charged and elementally balanced, the reactions extracted from the KEGG database needed to be examined for consistency and possibly modified before analysis was performed. The 357 reactions in the assembled gene insertion library were therefore subjected to charge and elemental balances. The charge balance for each candidate reaction was determined as follows:

$$b = R^T c \tag{10}$$

where c is a vector of charges for each species, R is the stoichiometric matrix assembled from all the candidate reactions, and b is the resulting vector of charge balances where a zero entry indicated a properly charge balanced reaction. A similar formulation was used to check elemental balances on hydrogen and carbon. Hydrogen ions were added to unbalanced reactions when the charge deficit matched the hydrogen deficit to simultaneously satisfy both balances. Six reactions were eliminated due to carbon imbalances, and 11 reactions were removed due to unsatisfied charge and/or hydrogen balances. Therefore, the final library consisted of 340 reactions corresponding to potential gene insertions. The same balancing procedure was applied to the eight reaction insertions proposed by Bro et al. (2006) to ensure consistency with the *i*ND750 model.

Table I. Model parameter values.

Variable	Value	References
$v_{o,max}$	8 mmol/gdw/h	Sonnleitner and Kappeli (1986)
K_o	0.003 mmol/L	Sonnleitner and Kappeli (1986)
O_{sat}	0.30 mmol/L	—
K_{ie}	10 g/L	—
V_0	0.5 L	—
V_f	1.2 L	—
X_0	0.05 g/L	—

Model Parameters and Dynamic Simulation

Nominal model parameter values used for all simulations are listed in Table I. Literature values for a wild-type yeast strain (Sonnleitner and Kappeli, 1986) were used for the oxygen uptake kinetic parameters ($v_{o,max}$, K_o). The saturation oxygen concentration (O_{sat}) was determined from Henry's law at 1.0 atm and 30°C. The initial and final volumes (V_0, V_f) and the initial biomass concentration (X_0) were chosen as representative values for a bench-scale bioreactor available in our laboratory. The glucose inhibition constant with respect to ethanol (K_{ie}) was chosen to give reasonable predictions of experimentally observed substrate, biomass and product profiles in batch culture with glucose (Jones and Kompala, 1999) and glucose/xylose (Kuyper et al., 2005) media. The sensitivity of the model predictions to this uncertain parameter is analyzed in the Results section. Additional model parameters needed for glucose media simulations are listed in Table II. The glucose uptake kinetic parameters ($v_{g,max}$, K_g) were obtained from the literature (Sonnleitner and Kappeli, 1986), while the feed flow rate (F), initial glucose concentration (G_0), glucose feed concentration (G_f), and final batch time (t_f) were chosen as representative values for our experimental system.

Table III lists parameter values specific to simulations of the xylose utilizing recombinant *S. cerevisiae* strain RWB 218 (Kuyper et al., 2005), including experimentally derived glucose and xylose uptake kinetic parameters. The fermenter operating conditions were chosen as representative values for our experimental system and equal concentrations of glucose and xylose in the media. Glucose and xylose are believed to be transported by the same family of hexose transporters with glucose being the preferred carbon source (Kuyper et al., 2005). The xylose inhibition constant with respect to glucose (K_{ig}) was chosen to capture the effect

Table II. Glucose media parameter values.

Variable	Value	References
$v_{g,max}$	20 mmol/gdw/h	Sonnleitner and Kappeli (1986)
K_g	0.5 g/L	Sonnleitner and Kappeli (1986)
F	0.044 L/h	—
G_f	100 g/L	—
t_f	16.0 h	—
G_0	10.0 g/L	—

Table III. Glucose and xylose media parameter values.

Variable	Value	References
$v_{g,max}$	7.3 mmol/gdw/h	Kuyper et al. (2005)
K_g	1.026 g/L	Kuyper et al. (2005)
$v_{z,max}$	32 mmol/gdw/h	Kuyper et al. (2005)
K_z	14.85 g/L	Kuyper et al. (2005)
K_{ig}	0.5 g/L	—
F	0.035 L/h	—
G_f	50 g/L	—
Z_f	50 g/L	—
t_f	20.0 h	—
G_0	5 g/L	—
Z_0	5 g/L	—

of repressed xylose uptake in the presence of glucose (Kuyper et al., 2005). The sensitivity of the model predictions to this uncertain parameter is analyzed in the Results section.

Dynamic simulations were performed in MATLAB using the code *ode23* to integrate the extracellular mass balance equations. The inner LP was evaluated inside the integration routine along with the dynamic equations using the MATLAB interface to the LP code MOSEK. A possible problem with FBA is the presence of multiple optimal solutions, which implies the existence of an infinite number of different flux distributions that produce the same optimal growth rate (Mahadevan and Schilling, 2003). Multiple optimal solutions with respect to the ethanol secretion rate were handled by first solving the LP (1) for maximum biomass, and then by fixing the biomass at this maximum value and resolving the LP for maximum ethanol secretion. This approach allowed variability in the ethanol production rate as a result of multiple optima to be eliminated by selecting the theoretical maximum ethanol production with respect to the maximal growth rate. Alternative approaches based on the solution of a mixed-integer LP (Lee et al., 2000) were deemed to be unnecessarily complex since only alternate optima with respect to the ethanol secretion rate were important for this study.

The ethanol productivity was defined as the overall rate of ethanol production from the fed-batch run:

$$\frac{(VE)|_{t=t_f}}{t_f} \tag{11}$$

where $t=0$ denotes the initial batch time. Dynamic optimization of fed-batch ethanol productivity was considered for two types of input profiles. In the first case the switching time between partially aerobic (50% *DO*; hereafter referred to as aerobic) and anaerobic conditions (0% *DO*) was treated as the only decision variable, while in the second case the *DO* concentration following the switch was treated as a second decision variable to investigate enhanced ethanol production under microaerobic conditions. For simplicity, a constant feed flow rate and feed substrate concentrations, fixed initial conditions, and a fixed final batch time were utilized in both cases. The resulting single and two variable optimization problems were solved with the MATLAB optimal search function *fminsearch*.

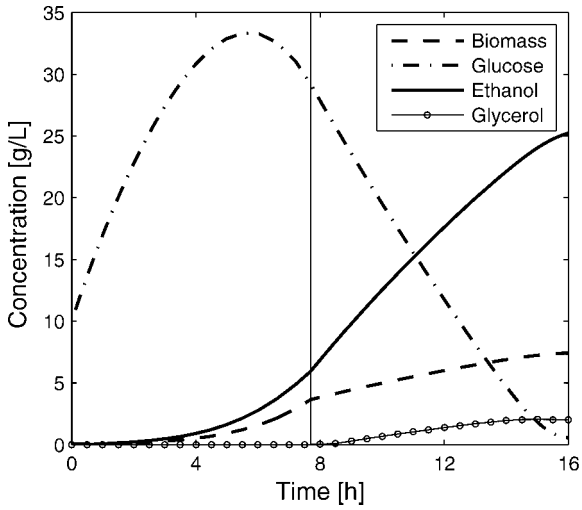

Figure 1. Fed-batch simulation profiles for wild-type *S. cerevisiae* with glucose feed and a switch in the dissolved oxygen concentration from 50% *DO* to 0% *DO* at 7.7 h indicated by the vertical line.

Results

Glucose Media

Fed-batch simulation of a constant glucose feed flow rate and an aerobic (50% *DO*) to anaerobic (0% *DO*) switch is shown in Figure 1. The initial conditions and parameter values for this simulation are reported in Tables I and II. A rapid increase in the biomass concentration was observed under aerobic growth conditions. The switch to anaerobic growth at 7.7 h resulted in a substantially increased ethanol production rate at the expense of biomass production. The final batch time obtained from solution of a full optimization problem (Hjersted and Henson, 2006) was extended slightly to compensate for the non-optimized glucose feeding strategy used in this study. The switching time (t_s) was chosen such that the glucose was nearly exhausted by the end of the batch. Competition between the byproduct glycerol and ethanol was observed after the switch to anaerobic conditions. The computational time for this dynamic simulation was only 9 s on a 3.0 GHz Pentium IV workstation.

The next set of results was generated from steady-state FBA of ten genetic manipulations for enhanced ethanol production suggested in Bro et al. (2006). Table IV shows in silico predictions for these manipulations along with results for the single gene deletion Δ*aac1*. The labels of the eight gene insertion strategies indicated in parentheses correspond to reaction entries in the KEGG LIGAND database.

DOI 10.1002/bit

Table IV. Steady-state FBA for glucose media.

Strategy	Inserted/overexpressed/deleted reaction	Ethanol yield increase (%)	Biomass yield increase (%)	Reaction flux (mmol/g/h)
	Anaerobic: Glucose uptake, $v_g = 5.0$ mmol g^{-1} h^{-1}, Oxygen uptake, $v_o = 0.0$ mmol g^{-1} h^{-1}			
Deletion of *gdh1* and overexpression of *glt1* and *gln1* (Δ*gdh1 glt1 gln1*)	2-Oxoglutarate + NH_4 + NADH + ATP → Glutamate + NAD + ADP	3.4	5.4	—
Deletion of gdh1 and overexpression of *gdh2* (Δ*gdh1 gdh2*)	2-Oxoglutarate + NH_4 + NADH → L-Glutamate + NAD	3.7	11.0	—
Insertion of NAD dependent glycine dehydrogenase (R00365)	Glyoxylate + NH_3 + NADH → Glycine + NAD + H_2O	3.8	18.0	1.18
Insertion of NADP dependent orotate reductase (R01866)	(S)-Dihydroorotate + NADP → Orotate + NADPH	3.9	18.1	1.20
Insertion of a transhydrogenase (R00112)	NADH + NADP → NADPH + NAD	3.8	18.0	1.18
Insertion of NADH kinase (R00105)	NADH + ATP → NADPH + ADP	6.1	5.6	0.87
Insertion of NADP dependent glycerol dehydrogenase (R01039)	Glycerol + NADP → Dihydroxyacetone + NADPH	6.1	5.6	0.88
Insertion of NADP dependent glycerol 3-phosphate dehydrogenase (R00845)	Glycerol 3-phosphate + NADP → D-glyceraldehyde 3-phosphate + NADPH	3.8	18.0	1.18
Insertion of NADP dependent glyceraldehyde-3-phosphate dehydrogenase (R01063)	D-Glyceraldehyde 3-phosphate + NADP + P → 3-phospho-D-glyceroyl phosphate + NADPH	3.8	18.0	1.18
Insertion of non-phosphorylating NADP dependent glyceraldehyde-3-phosphate dehydrogenase (e.g., *gapN*; R01058)	D-Glyceraldehyde 3-phosphate + NADP → 3-phospho-D-glycerate + NADPH	6.1	5.6	0.87
Deletion of *aac1* (Δ*aac1*)	ADP[c] + ATP[m] → ADP[m] + ATP[c]	0.0	0.0	—
	Wild-type: growth rate, $\mu = 0.085$ h^{-1}, ethanol yield, $Y_{e/g} = 0.424$ g/g			
	Aerobic:[a] Glucose uptake, $v_g = 5.0$ mmol g^{-1} h^{-1}, Oxygen uptake, $v_o = 7.84$ mmol g^{-1} h^{-1}			
Deletion of *gdh1* and overexpression of *glt1* and *gln1* (Δ*gdh1 glt1 gln1*)	2-Oxoglutarate + NH_4 + NADH + ATP → Glutamate + NAD + ADP	9.5	−7.4	—
Deletion of *aac1* (Δ*aac1*)	ADP[c] + ATP[m] → ADP[m] + ATP[c]	76.4	−59.9	—
	Wild-type: growth rate, $\mu = 0.339$ h^{-1}, ethanol yield, $Y_{e/g} = 0.166$ g/g			

[a]Aerobic yields differed from the wild-type only for the two strategies reported.

The genetic manipulation strategies are subsequently referred to by these labels. The modifications of the insertion reactions needed to achieve charge and elemental balancing are shown explicitly in the Appendix. LPs for both anaerobic (0% *DO*) and aerobic (50% *DO*) conditions were solved for each manipulation. All manipulations produced enhanced ethanol and growth yields for anaerobic growth with the exception of Δ*aac1*, which corresponds to a flux in oxidative phosphorylation that is only active aerobically. The flux through each inserted reaction was significant compared to the glucose uptake rate. Under aerobic conditions, only two manipulations generated ethanol and biomass yields that differed from the wild-type. Enhanced aerobic ethanol production at the expense of reduced cellular growth was predicted for both of these strategies.

In the original study of Bro et al. (2006), anaerobic yield enhancements of 4.2–10.4% for ethanol and 5.2–16.5% for biomass were predicted for their ten proposed manipulations. When these predictions were compared to the FBA results in Table IV, particularly large differences were observed in the ethanol yields. These differences were attributable to the different flux balance models analyzed in the two studies. We believe that the additional compartmentalization and full charge balancing of the *i*ND750 model used in this study were the primary causes of the discrepancies with the *i*FF708 model (Forster et al., 2003) used in the original study. The lower ethanol yield predictions from the *i*ND750 model seemed to be more consistent with experimental data, but both models overpredicted experimentally observed growth rates (Bro et al., 2006).

The results in Table IV demonstrated a notable shortcoming of classical FBA. Given different relative enhancements in anaerobic ethanol and biomass yields, the preferred manipulation for aerobic ethanol production could not be directly determined. A similar difficulty was encountered for aerobic growth, where the impact of increased ethanol yield and decreased biomass yield for the two manipulations listed could not be quantitatively compared to the wild-type with respect to total ethanol production. Consequently, the preferred manipulation for fed-batch ethanol production in which an aerobic growth phase is followed by an anaerobic growth phase could not be determined without further analysis.

We defined the ethanol productivity as the total mass of ethanol produced divided by the duration of the batch. The productivity represents a single measure of fed-batch performance that explicitly incorporates the tradeoff between time-varying ethanol and biomass yields throughout the batch. DFBA results for the sensitivity of the ethanol productivity to the aerobic-anaerobic switching time in fed-batch culture are shown in Figure 2. These results were generated for each manipulation strategy by repeated fed-batch simulation with different switching times. The initial conditions and parameter values used are reported in Tables I and II. The maximal productivities shown as peaks

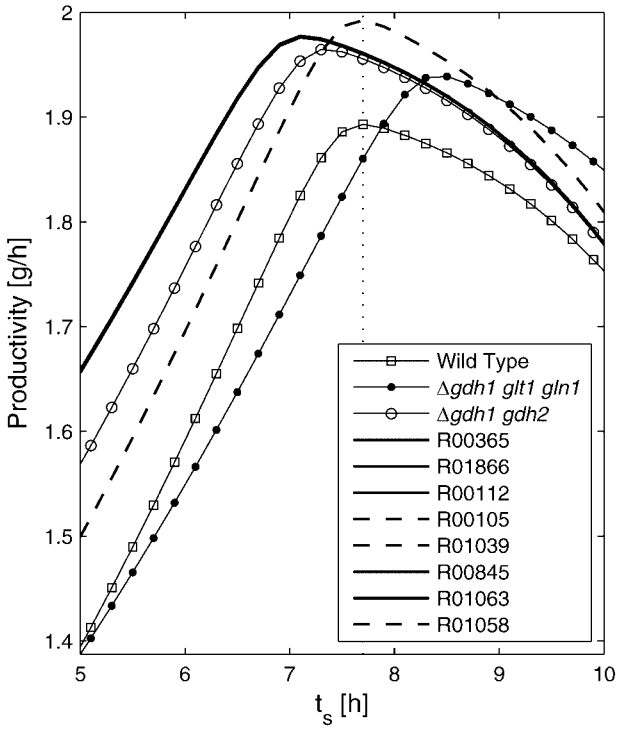

Figure 2. Sensitivity of the ethanol productivity to the aerobic–anaerobic switching time (t_s) in fed-batch culture with glucose media. The dotted line indicates the optimal switching time for the wild-type strain.

in Figure 2 could be used to produce an explicit ranking of the manipulation strategies: (1) R00105/R01039/R01058; (2) R00365/R01866/R00112/R00845/R01063; (3) Δ*gdh1 gdh2*; (4) Δ*gdh1 glt1 gln1*; (5) wild-type. The reduced growth yield of the deletion strategy Δ*aac1* overwhelmed the increased ethanol yield, generating productivities below the scale in Figure 2. The vertical dotted line at the optimal productivity for the wild-type strain demonstrates that the manipulation strategies have different optimal switching times. Consequently, optimal performance is dependent both on the metabolic engineering strategy and the fed-batch operating policy. This suggests that attempts to separately optimize the cellular design and the fermentation conditions are likely to produce suboptimal ethanol productivities.

Single variable optimization was performed to confirm the optimal switching times found in the sensitivity analysis (Fig. 2). Simultaneous optimization of the switching time and the dissolved oxygen concentration (*DO*) following the switch was also conducted to investigate enhanced fed-batch productivity under microaerobic conditions. The two variable optimization problem required about 18 min of computation time for each manipulation strategy. The results in Table V show that each manipulation except Δ*aac1*

DOI 10.1002/bit

Table V. Fed-batch optimization for glucose media.

Label	t_s (h)	Productivity increase (%)[a]	t_s (h)	DO_s (%)	Productivity increase (%)[a]	Microaerobic increase (%)[b]
R00105	7.66	5.25	7.43	0.019	2.09	0.09
R01039	7.66	5.25	7.43	0.019	2.09	0.09
R01058	7.66	5.25	7.43	0.019	2.09	0.09
R01866	7.13	4.46	6.83	0.031	1.64	0.40
R00365	7.13	4.38	6.83	0.031	1.64	0.47
R00112	7.13	4.38	6.83	0.031	1.64	0.47
R00845	7.13	4.38	6.83	0.031	1.64	0.47
R01063	7.13	4.38	6.83	0.031	1.64	0.47
Δ*gdh1 gdh2*	7.35	3.79	6.94	0.031	1.70	1.12
Δ*gdh1 glt1 gln1*	8.40	2.46	8.10	0.033	1.18	1.90
Δ*aac1*	14.09	−29.74	12.95	0.099	−29.96	2.86
Wild-type	7.70	1.89 g/h	6.94	0.079	1.95 g/h	3.19

[a]Productivity increase over wild-type (actual wild-type productivity reported in last row).
[b]Microaerobic productivity increase over a purely anaerobic phase for the same strategy.

was predicted to outperform the wild-type. Although not the focus of this study, the very low *DO* concentrations listed would be difficult to achieve experimentally. The largest productivity enhancement under microaerobic conditions versus purely anaerobic conditions was predicted for the wild-type (3.19%), whereas the manipulations with the highest productivity under anaerobic conditions yielded the smallest predicted benefit (0.09%) from microaerobic growth. However, the relative ranking of the manipulation strategies remained mostly unchanged under microaerobic growth with the notable exception that the deletion/overexpression strategy Δ*gdh1 ghd2* slightly outperformed five insertion strategies that were previously ranked higher. This result provides another illustration of the need to consider the design of metabolic engineering strategies and process operating policies simultaneously. The deletion strategy Δ*aac1* was omitted from further analysis due to its poor performance.

The sensitivity of optimal fed-batch productivities to the glucose inhibition constant with respect to ethanol (K_{ie}) was examined to assess the impact of this uncertain parameter. Results are shown in Figure 3 for each manipulation strategy, where the dotted line represents the nominal parameter value. A point on this plot was generated by fixing the genetic manipulation and the K_{ie} value and then optimizing the aerobic–anaerobic switching time to determine the maximal productivity. For each manipulation, the productivity dropped sharply below the nominal value and leveled off at larger values where inhibition had a diminished effect. The relative rankings of the manipulations were mostly unchanged by the K_{ie} value. However a crossing of the wild-type and the Δ*gdh1 glt1 gln1* curves was observed near $K_{ie} = 6$ g/L because the inhibitory effect of ethanol is increased at small K_{ie} values.

Glucose and Xylose Media

We conducted dynamic simulations for fed-batch fermentation with 50%/50% glucose/xylose mixtures using the parameter values and initial conditions reported in Tables I and III. To our knowledge, this study represents the first application of DFBA to mixed substrates. Compared to the glucose media results reported earlier, the results shown in Figure 4 were generated with a longer final batch time of 20 h due to the xylose utilizing strain having higher saturation constants, a lower maximum glucose uptake rate, and inhibition of xylose uptake in the presence of glucose. Furthermore, a longer aerobic phase was necessary to generate a sufficiently high biomass concentration such that most of the substrate was consumed by the final batch time. The switch from aerobic to anaerobic conditions at 16 h was characterized by a significant increase in ethanol production and a sharp decline in biomass production. The xylose

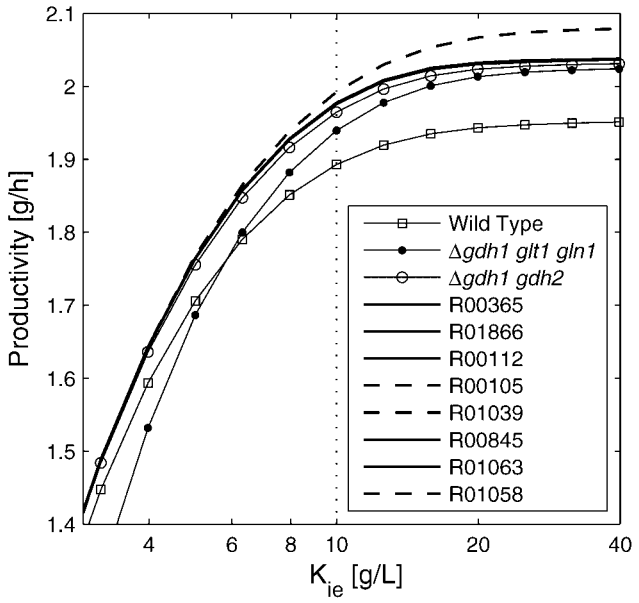

Figure 3. Sensitivity of the fed-batch ethanol productivity to the inhibition constant K_{ie} for glucose media. The dotted line indicates the nominal parameter value.

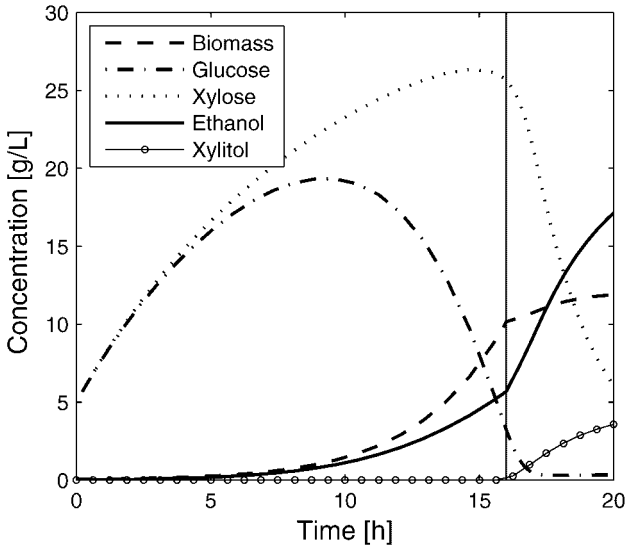

Figure 4. Fed-batch simulation profiles for the xylose utilizing *S. cerevisiae* strain RWB 218 (Kuyper et al., 2005) with glucose and xylose feed and a switch in the dissolved oxygen concentration from 50% *DO* to 0% *DO* at 17.0 h indicated by the vertical line.

concentration increased due to feeding until decreasing sharply after glucose was nearly exhausted. Glycerol production was insignificant as a result of the limited residual glucose present following the switch to anaerobic conditions. The production rate of the byproduct xylitol was much higher than was the competing byproduct glycerol in the glucose media case (Fig. 1), which suggested that metabolic engineering strategies are needed to divert carbon from xylitol to ethanol and/or biomass. These fed-batch predictions are in reasonable agreement with experimental batch profiles presented in Kuyper et al. (2005).

Steady-state FBA results with mixed substrates are presented in Table VI for the ten genetic manipulations suggested by Bro et al. (2006). While each manipulation was predicted to yield a simultaneous increase in the ethanol and biomass yields under anaerobic conditions compared to the wild-type, the relative performance of these manipulations could not be determined without further analysis. Compared to glucose media (Table IV), higher increases in ethanol yields and smaller increases in biomass yields were predicted. The flux through each inserted reaction was significant, ranging between 18% and 41% of the glucose uptake rate. Only the deletion/overexpression Δ*gdh1 glt1 gln1* differed from the wild-type under aerobic conditions (50% *DO*). The performance impact of the substantial increase in ethanol yield and the large decrease in biomass yield was difficult to assess, especially when considering fed-batch culture with both aerobic and anaerobic growth phases.

The sensitivity of fed-batch ethanol productivities with mixed substrate to the aerobic-anaerobic switching time is shown in Figure 5. Parameter values and initial conditions used are listed in Tables I and III. The predicted productivities were substantially lower than for glucose media (Fig. 2) due to differences in the substrate uptake kinetics and to significant secretion of xylitol as a competing byproduct. The productivity measure allowed an explicit ranking of the manipulation strategies, with the R00112, R00365, R00845, R01063, and R01866 insertions predicted to yield the best performance. These insertions comprised the second highest ranked group for glucose media, demonstrating that the media should be considered simultaneously with the genetic manipulation and the fed-batch operating policy to achieve optimal performance. Unlike glucose media (Fig. 2) the optimal switching time was relatively insensitive to the manipulation, indicating that the optimal switching time was most strongly affected by the substrate uptake kinetics. Only the deletion/overexpression Δ*gdh1 glt1 gln1* required a significantly

Table VI. Steady-state FBA for glucose and xylose media.

Label	Ethanol yield increase (%)	Biomass yield increase (%)	Reaction flux (mmol/g/h)
	Anaerobic: $v_g = 2.4$, $v_z = 2.1$, $v_o = 0.0$ (mmol/g/h)		
Δ*gdh1 glt1 gln1*	9.1	4.1	—
Δ*gdh1 gdh2*	8.1	9.5	—
R00365	12.2	15.2	0.96
R01866	12.3	15.3	0.98
R00112	12.2	15.2	0.96
R00105	9.6	4.1	0.44
R01039	9.6	4.1	0.45
R00845	12.2	15.2	0.96
R01063	12.2	15.2	0.96
R01058	9.6	4.1	0.45
	Wild-type: $\mu = 0.085\ h^{-1}$, $Y_{e/g} = 0.424$ g/g		
	Aerobic:[a] $v_g = 2.4$, $v_z = 2.1$, $v_o = 7.84$ (mmol/g/h)		
Δ*gdh1 glt1 gln1*	17.7	−7.6	—
	Wild-type: $\mu = 0.339\ h^{-1}$, $Y_{e/g} = 0.166$ g/g		

[a]Aerobic yields differed from the wild-type only for the single strategy reported.

DOI 10.1002/bit

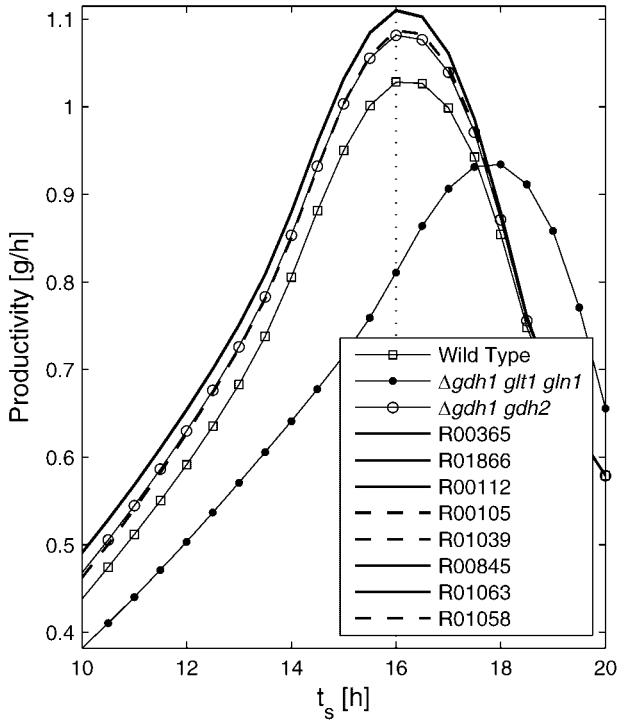

Figure 5. Sensitivity of the ethanol productivity to the aerobic–anaerobic switching time (t_s) in fed-batch culture with glucose and xylose media. The dotted line indicates the optimal switching time for the wild-type strain.

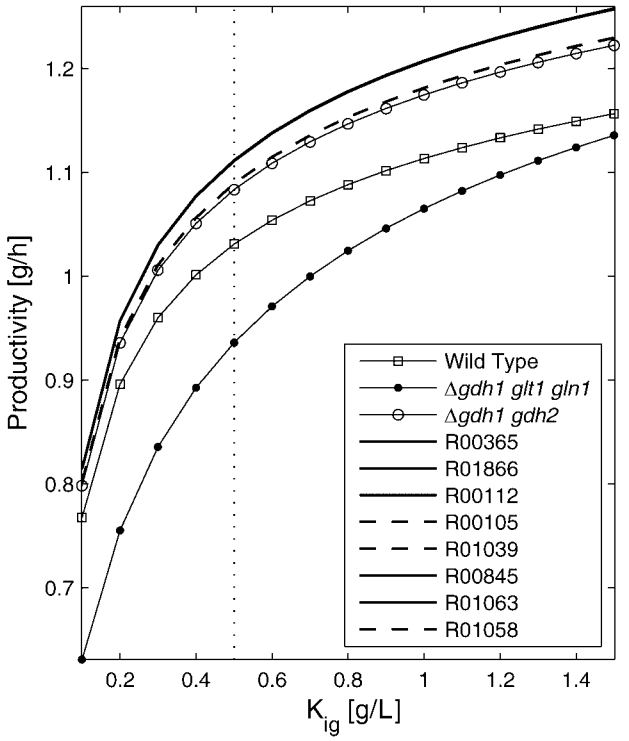

Figure 6. Sensitivity of the fed-batch ethanol productivity to the inhibition constant K_{ig} for glucose and xylose media. The dotted line indicates the nominal parameter value.

different switching time, but this manipulation produced a substantially lower productivity due to its reduced biomass yield. Comparison of these dynamic predictions with the steady-state FBA results (Table VI) revealed that manipulations with relatively high biomass yields were most favorable in fed-batch culture. Tests with 25%/75% and 75%/25% glucose/xylose mixtures were conducted and similar trends were predicted (not shown).

We investigated the sensitivity of the optimal fed-batch productivities to the xylose uptake inhibition constant with respect to glucose (K_{ig}) to assess the impact of this uncertain model parameter. Figure 6 shows that the ethanol productivities declined sharply below the nominal parameter value and increased approximately linearly at larger values. However, the relative productivities of the ten manipulation strategies remained roughly constant over a wide range of K_{ig} values. Therefore, an accurate value for K_{ig} was not needed to rank the manipulations according to their relative fed-batch performance. Sensitivity to the final batch time was also tested, and the overall rank of the manipulation strategies remained unchanged over a large range of t_f values (not shown). The relative performance of the strategies was also insensitive to the final batch time with the exception of Δ*gdh1 glt1 gln1*, which performed better than the wild-type at longer batch times but still underperformed all the other strategies.

Dynamic Screening of the KEGG Ligand Library

The ten genetic manipulations suggested by Bro et al. (2006) were identified through classical FBA. In the previous two subsections, we subjected these manipulations to further screening with DFBA. Our results demonstrated that steady-state analysis alone was inadequate for screening manipulations according to their achievable fed-batch performance where dynamic effects are critical. Therefore, we investigated the possibility that novel gene insertions for ethanol overproduction in fed-batch culture could be identified directly through dynamic analysis.

As explained in the Methods section, we assembled a set of 340 candidate gene insertions from the KEGG Ligand database by subjecting cytosolic reactions to charge, hydrogen and carbon balancing to allow their direct incorporation into the *i*ND750 metabolic reconstruction. First the fed-batch performance of each candidate insertion was assessed by optimizing the aerobic–anaerobic switching time to determine maximal ethanol productivity under the assumption of reaction reversibility due to lack of such information in the KEGG database. Promising insertions were further scrutinized if the reverse reaction direction was used either aerobically or anaerobically. In addition to examining the available literature on *S. cerevisiae*, we checked other genome-scale models for reactions corresponding to gene insertion

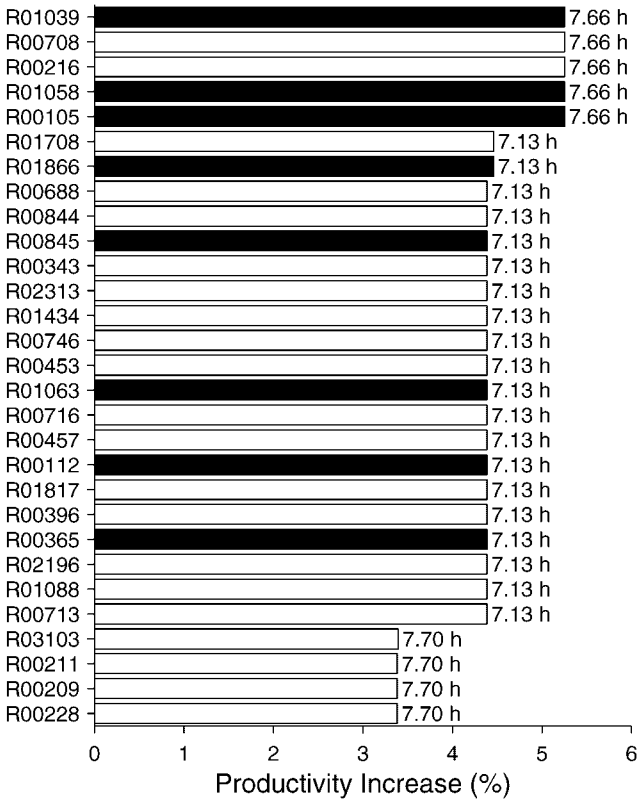

Figure 7. Dynamic screening of a gene insertion library derived from the KEGG database for optimal fed-batch ethanol productivity with glucose media. Insertions proposed by Bro et al. (2006) are shown as black bars. The number indicated to the right of each bar indicates the optimal aerobic–anaerobic switching time.

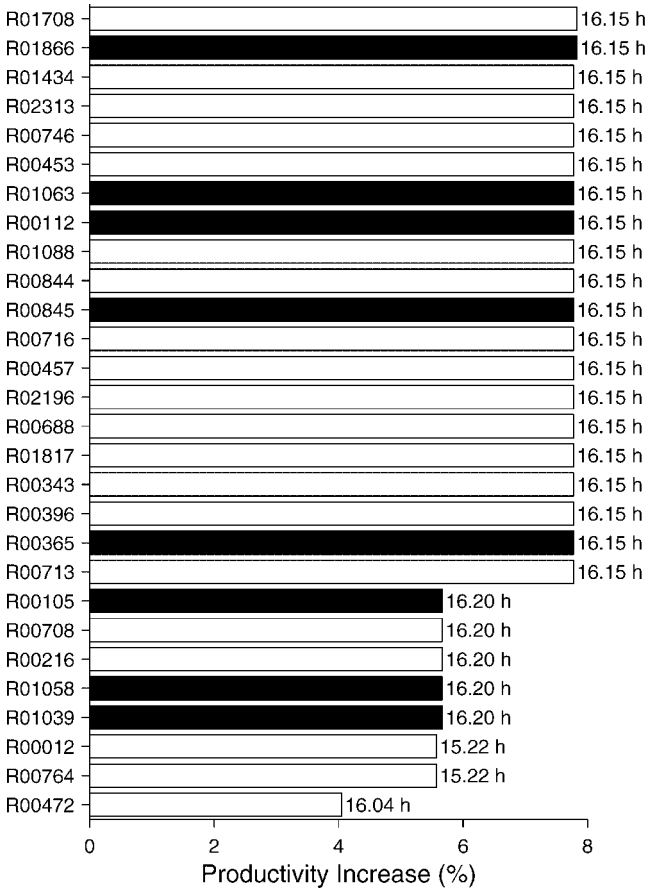

Figure 8. Dynamic screening of a gene insertion library derived from the KEGG database for optimal fed-batch ethanol productivity with glucose and xylose media. Insertions proposed by Bro et al. (2006) are shown as black bars. The number indicated to the right of each bar indicates the optimal aerobic–anaerobic switching time.

candidates natively found in those species (Reed et al., 2006). If available data suggested that a particular inserted reaction was irreversible, fed-batch optimization was repeated with the corresponding flux appropriately constrained.

Figure 7 shows the dynamic screening results for glucose media where the eight insertions suggested by Bro et al. (2006) are indicated by black bars. The insertions are labeled by their entries in the KEGG LIGAND database and the corresponding reactions are listed in the Appendix. In addition to the eight previously analyzed insertions, the procedure identified 21 new insertion strategies with productivity enhancements greater than 3% over the wild-type value. The insertions could be grouped into three sets, each with the same aerobic–anaerobic switching time and very similar productivities. The switching time varied only slightly between these three groups. The two new candidate insertions with the highest productivities correspond to expression of a NADP-specific 1-pyrroline-5-carboxylate dehydrogenase (R00708) and a NADP-malic enzyme (R00216). A NAD-specific 1-pyrroline-5-carboxylate and the same NADP-malic enzyme are already expressed in the mitochondria, so identification of these cytosolic insertions required a compartmentalized metabolic network model. Both of the proposed insertions maintain a favorable redox balance for ethanol production by generating NADPH, and therefore they represent similar design alternatives to those previously proposed (Bro et al., 2006).

Dynamic screening results for glucose and xylose media are shown in Figure 8. As with glucose media, insertions that yielded ethanol productivity enhancements larger than 3% of the wild-type value were analyzed in more detail. The dynamic screen revealed 15 new insertions that matched the performance of the top five insertions from Bro et al. (2006). The top 25 insertions could be divided into two sets according to their optimal switching time and predicted ethanol productivity. These two sets appeared in both the glucose and mixed-media screens, but their relative performance was reversed such that the top 5 insertions from the glucose media screen were surpassed by the set of 20 insertions in the mixed-media screen. This result emphasizes the importance of explicitly considering the

DOI 10.1002/bit

media composition when utilizing DFBA to identify mutants for metabolite overproduction.

Discussion

A dynamic flux balance model based on a genome-scale reconstruction of *S. cerevisiae* was developed to analyze cellular metabolism and ethanol production in fed-batch culture. The problem of maximizing ethanol productivity in glucose and glucose/xylose media was addressed by computing optimal aerobic–anaerobic switching times for candidate metabolic engineering strategies. The first set of ten genetic manipulations considered was proposed by Bro et al. (2006) through the application of steady-state FBA. These manipulations were subjected to an additional round of DFBA in which optimal fed-batch ethanol productivities were computed to assess possible limitations of steady-state FBA. A more comprehensive set of gene insertion candidates generated from the KEGG LIGAND database allowed direct DFBA screening for achievable ethanol overproduction in fed-batch culture.

Our dynamic flux balance model was based on the genome-scale reconstruction *i*ND750 (Duarte et al., 2004), which is an improved version of the *i*FF708 reconstruction (Forster et al., 2003) used by Bro et al. (2006) for their steady-state FBA. When FBA was performed with the *i*ND750 model, we obtained significantly lower ethanol yields than in the original study. The *i*ND750 model includes full compartmentalization and charge balancing, and as a result the reactions present in *i*FF708 only comprise 56% of the total reactions in *i*ND750. While the precise causes of the observed discrepancies were not determined, an analysis of reactions inserted with and without proper charge balancing revealed that model predictions were sensitive to charge balances (not shown). Because *i*ND750 has more detailed charge balancing and yields predictions in better agreement with data (Bro et al., 2006), we believe that *i*ND750 is a superior metabolic reconstruction for evaluating ethanol overproduction strategies that are inherently sensitive to the global redox balance.

While providing valuable information about metabolic engineering strategies, FBA was shown to have several shortcomings that limit its applicability to metabolite overproduction studies in dynamic cell culture. The productivity of growth associated metabolites such as ethanol is determined both by the biomass yield and the metabolite yield, and tradeoffs between these two measures are not easily handled within the FBA framework. This problem is exasperated in batch and fed-batch culture due to dynamic effects that result in time varying yields. Consequently, genetic manipulations for optimal ethanol production in fed-batch culture where an aerobic growth phase is followed by an anaerobic growth phase cannot be directly determined without further analysis. DFBA addresses this problem by embedding stoichiometric equations of intracellular metabolism within transient mass balances on the extracellular environment, thereby providing dynamic predictions of extracellular metabolite concentrations. We extended the DFBA framework to allow the integrated design of metabolic engineering strategies and fed-batch operating policies by computing optimal aerobic-anaerobic switching times that maximized ethanol production for candidate genetic alterations. While more computationally demanding than FBA, our DFBA procedure allowed an explicit ranking of candidate strategies according to their predicted ethanol productivity in fed-batch culture.

Our DFBA results for glucose media showed that the ten genetic manipulations of Bro et al. (2006) produced different fed-batch ethanol productivities and that the aerobic–anaerobic switching times were dependent on the gene deletion/overexpression/insertion used. Small additional improvements in ethanol productivities were predicted when microaerobic growth was allowed following the switch from the aerobic phase. The predicted productivities were sensitive to the parameter for glucose uptake inhibition with respect to ethanol (K_{ie}) as evidenced by a rearrangement in the relative performance of the wild-type strain and a gene overexpression/deletion strategy occurring at a particular K_{ie} value.

A desirable feature of the DFBA framework is that additional substrates and products can be included by adding the necessary extracellular mass balances and substrate uptake expressions to the dynamic flux balance model. We showed that DFBA could be applied to mixed substrates by investigating the achievable fed-batch ethanol productivities of the Bro et al. (2006) manipulations in glucose and xylose media. A rearrangement of the most favorable manipulations compared to the glucose media results was observed, demonstrating that the media is a critical factor in metabolic engineering for fed-batch ethanol production. This reordering suggested that a direct dynamic screen of candidate genetic manipulations for mixed substrates should be conducted to avoid omitting promising strategies. While predicted productivities were sensitive to the parameter for xylose uptake inhibition with respect to glucose (K_{ig}), the relative performance obtained with the ten manipulations was not affected by the parameter value.

To explore the possibility that novel gene insertions for ethanol overproduction in fed-batch culture could be identified directly with DFBA, we assembled a library of 340 candidate reactions from the KEGG Ligand database. Each reaction was charge, carbon, and hydrogen balanced to ensure consistency with the *i*ND750 metabolic reconstruction. Dynamic screening of the library for optimal fed-batch performance in glucose media revealed two novel insertions that produced the same ethanol productivity as the three highest ranked manipulations of Bro et al. (2006), while the mixed-media screen revealed 15 new insertions with the same ethanol productivity as predicted for the top 5 insertions proposed by Bro et al. (2006). The metabolic engineering strategies identified through direct DFBA represent alternative and potentially more easily implementable targets for experimental evaluation.

Collectively, the results reported in this paper demonstrate the potential power of DFBA for in silico metabolic engineering of batch and fed-batch microbial cultures. This initial study motivates several possible enhancements of the DFBA framework. In our current formulation, the only mechanism for incorporating known regulatory effects is through the substrate uptake expressions. Previous work with classical FBA has shown that gene expression data can be used to constrain regulated fluxes within genome-scale metabolic networks (Åkesson et al., 2004; Covert et al., 2001). The incorporation of such data within the DFBA framework is more challenging due to the difficulty of using steady-state snapshots of gene expression to constrain an inherently dynamic model.

We showed that previously proposed metabolic engineering strategies and libraries of candidate single gene insertions could be dynamically screened through a brute force strategy involving enumeration and evaluation. Because this approach may be infeasible for screening large libraries and/or multiple gene insertions, extensions of existing mixed-integer linear programming methods (Burgard and Maranas, 2001; Pharkya et al., 2004) that account for culture dynamics are needed. We computed optimal fed-batch operating policies by considering the dissolved oxygen switching time and the post-switch dissolved oxygen concentration as the only decision variables under the assumption of constant substrate feeding. A more complete strategy would allow optimization of the initial batch conditions, the substrate feeding policies, and the final batch time. Our initial work with small-scale dynamic flux balance models (Hjersted and Henson, 2006) suggests that this goal is also achievable for genome-scale flux models. Ultimately, computational strategies that allow simultaneous optimization of the cellular design, media components, and dynamic operating policies for maximization of metabolite production in batch and fed-batch culture should be developed. Our future work will focus on incorporating dynamic regulation, developing more sophisticated optimization strategies, and experimental model validation and mutant strain evaluation.

Appendix

Label	EC	Reaction
R00012	2.7.7.45	2 GTP + H+ ⇔ P4-Bis(5′-guanosyl) tetraphosphate + Diphosphate
R00105	2.7.1.86	ATP + NADH ⇔ ADP + H+ + NADPH
R00112	1.6.1.1	NAD + NADPH ⇔ NADH + NADP
R00209	1.2.1.51	CoA + NAD + Pyruvate ⇔ Acetyl-CoA + CO_2 + NADH
R00211	1.2.3.6	CoA + H+ + O_2 + Pyruvate ⇔ Acetyl-CoA + CO_2 + $H2O_2$
R00216	1.1.1.40	L-Malate + NADP → O_2 + NADPH + Pyruvate
R00228	1.2.1.10	Acetaldehyde + CoA + NAD ⇔ Acetyl-CoA + H+ + NADH
R00343	1.1.1.82	L-Malate + NADP ⇔ H+ + NADPH + Oxaloacetate
R00365	1.4.1.10	Glycine + H_2O + NAD ⇔ Glyoxylate + H+ + NADH + NH_4
R00396	1.4.1.1	L-Alanine + H_2O + NAD ⇔ H+ + NADH + NH_4 + Pyruvate
R00453	2.6.1.71	L-Lysine + Pyruvate ⇔ L-2-Aminoadipate 6-semialdehyde + L-Alanine
R00457	2.6.1.36	2-Oxoglutarate + L-Lysine ⇔ L-2-Aminoadipate 6-semialdehyde + L-glutamate
R00472	2.3.3.9	CoA + H+ + L-Malate ⇔ Acetyl-CoA + Glyoxylate + H_2O
R00688	1.4.1.20	H_2O + NAD + L-Phenylalanine ⇔ H+ + NADH + NH_4 + Phenylpyruvate
R00708	1.5.1.12	1-Pyrroline-5-carboxylate + 2 H_2O + NADP → L-Glutamate + H+ + NADPH
R00710	1.2.1.3	Acetaldehyde + H_2O + NAD ⇔ Acetate + 2 H+ + NADH
R00713	1.2.1.24	H_2O + NAD + Succinic semialdehyde ⇔ 2 H+ + NADH + Succinate
R00716	1.5.1.8	H_2O + NADP + L-Saccharopine ⇔ 2-Oxoglutarate + H+ + L-Lysine + NADPH
R00746	1.1.1.2	Ethanol + NADP ⇔ Acetaldehyde + H+ + NADPH
R00764	2.7.1.90	D-Fructose 6-phosphate + Diphosphate ⇔ D-Fructose 1,6-bisphosphate + H+ + Phosphate
R00844	1.1.1.94	Glycerol 3-phosphate + NADP ⇔ Dihydroxyacetone phosphate + H+ + NADPH
R00845	1.1.1.177	Glycerol 3-phosphate + NADP ⇔ Glyceraldehyde 3-phosphate + H+ + NADPH
R01039	1.1.1.156	Glycerol + NADP ⇔ Dihydroxyacetone + H+ + NADPH
R01058	1.2.1.9	Glyceraldehyde 3-phosphate + H_2O + NADP → 3-Phospho-D-glycerate + 2 H+ + NADPH
R01063	1.2.1.13	Glyceraldehyde 3-phosphate + NADP + Phosphate ⇔ 3-Phospho-D-glyceroyl phosphate + H+ + NADPH
R01088	1.4.1.9	H_2O + L-Leucine + NAD ⇔ 4-Methyl-2-oxopentanoate + H+ + NADH + NH_4
R01434	1.4.1.9	H_2O + NAD + L-Valine ⇔ 3-Methyl-2-oxobutanoate + H+ + NADH + NH_4
R01708	1.1.1.65	NADP + Pyridoxine ⇔ H+ + NADPH + Pyridoxal
R01817	1.1.1.224	D-Mannitol 1-phosphate + NADP ⇔ H+ + D-Mannose 6-phosphate + NADPH
R01866	1.3.1.15	(S)-Dihydroorotate + NADP ⇔ H+ + NADPH + Orotate
R02196	1.4.1.9	H2O + L-Isoleucine + NAD ⇔ (S)-3-Methyl-2-oxopentanoate + H+ + NADH + NH_4
R02313	1.5.1.9	H_2O + NAD + L-Saccharopine ⇔ L-2-Aminoadipate 6-semialdehyde + L-Glutamate + H+ + NADH
R03103	1.2.1.31	L-2-Aminoadipate 6-semialdehyde + H_2O + NADP ⇔ L-2-Aminoadipate + 2 H+ + NADPH

DOI 10.1002/bit

Nomenclature

DO	dissolved oxygen concentration [%]
E	ethanol concentration [g/L]
F	feed flowrate [L/h]
G	glucose concentration [g/L]
G_f	feed glucose concentration [g/L]
K_{ie}	glucose uptake inhibition constant with respect to ethanol [g/L]
K_{ig}	xylose uptake inhibition constant with respect to glucose [g/L]
K_g	glucose uptake saturation constant [g/L]
K_o	oxygen uptake saturation constant [mmol/L]
K_z	xylose uptake saturation constant [g/L]
O	liquid oxygen concentration [mmol/L]
O_{sat}	saturation liquid oxygen concentration [mmol/L]
V	liquid volume [L]
X	biomass concentration [g/L]
Z	xylose concentration [g/L]
Z_f	feed xylose concentration [g/L]
ν_e	ethanol exchange rate [mmol/gdw/h]
ν_g	glucose uptake rate [mmol/gdw/h]
ν_o	oxygen uptake rate [mmol/gdw/h]
ν_z	xylose uptake rate [mmol/gdw/h]
μ	specific growth rate [h^{-1}]

References

Åkesson M, Forster J, Nielsen J. 2004. Integration of gene expression data into genome-scale metabolic models. Metabol Eng 6:285–293.

Aristidou A, Penttila M. 2000. Metabolic engineering applications to renewable resource utilization. Curr Opin Biotechnol 11:187–198.

Bro C, Regenberg B, Forster J, Nielsen J. 2006. In silico aided metabolic engineering of Saccharomyces cerevisiae for improved bioethanol production. Metabolic Eng 8:102–111.

Burgard AP, Maranas CD. 2001. Probing the performance limits of the Escherichia coli metabolic network subject to gene additions or deletions. Biotechnol Bioeng 74:364–375.

Covert MW, Schilling CH, Palsson BO. 2001. Regulation of gene expression in flux balance models of metabolism. J Theor Biol 213: 73–88.

Duarte NC, Herrgard MJ, Palsson BO. 2004. Reconstruction and validation of Saccharomyces cerevisiae iND750, a fully compartmentalized genome-scale metabolic model. Genome Res 14:1298–1309.

Famili I, Forster J, Nielsen J, Palsson BO. 2003. Saccharomyces cerevisiae phenotypes can be predicted by using constraint-based analysis of a genome-scale reconstructed metabolic network. Proc Natl Acad Sci USA 100:13134–13139.

Forster J, Famili I, Fu P, Palsson BO, Nielsen J. 2003. Genome-scale reconstruction of the Saccharomyces cerevisiae metabolic network. Genome Res 13:244–253.

Gadkar KP, Doyle FJ III, Edwards JS, Mahadevan R. 2004. Estimating optimal profiles of genetic alterations using constraint-based models. Biotechnol Bioeng 89:243–251.

Giaever G, Chu AM, Ni L, Connelly C, Riles L, Véronneau S, Dow S, Lucau-Danila A, Anderson K, André B, Arkin AP, Astromoff A, Bakkoury ME, Bangham R, Benito R, Brachat S, Campanaro S, Curtiss M, Davis K, Deutschbauer A, Entian KD, Flaherty P, Foury F, Garfinkel DJ, Gerstein M, Gotte D, Güldener U, Hegemann JH, Hempel S, Herman Z, Jaramillo DF, Kelly DE, Kelly SL, Kötter P, LaBonte D, Lamb DC, Lan N, Liang H, Liao H, Liu L, Luo C, Lussier M, Mao R, Menard P, Ooi SL, Revuelta JL, Roberts CJ, Rose M, Ross-Macdonald P, Scherens B, Schimmack G, Shafer B, Shoemaker DD, Sookhai-Mahadeo S, Storms RK, Strathern JN, Valle G, Voet M, Volckaert G, Wang C, Ward TR, Wilhelmy J, Winzeler EA, Yang Y, Yen G, Youngman E, Yu K, Bussey H, Boeke JD, Snyder M, Philippsen P, Davis RW, Johnston M. 2002. Functional profiling of the Saccharomyces cerevisiae genome. Nature 418:387–391.

Hatzimanikatis V, Emmerling M, Sauer U, Bailey JE. 1998. Application of mathematical tools for metabolic design of microbial ethanol production. Biotech Bioeng 58:154–161.

Hjersted JL, Henson MA. 2006. Optimization of fed-batch Saccharomyces cerevisiae fermentation using dynamic flux balance models. Biotechnol Prog 22:1239–1248.

Jeffries TW, Jin YS. 2004. Metabolic engineering for improved fermentation of pentoses by yeasts. Appl Microbiol Biotechnol 63:495–509.

Jones KD, Kompala DS. 1999. Cybernetic modeling of the growth dynamics of Saccharomyces cerevisiae in batch and continuous cultures. J Biotech 71:105–131.

Kanehisa M. 1997. A database for post-genome analysis. Trends Genet 13:375–376.

Kanehisa M, Goto S. 2000. KEGG: Kyoto encyclopedia of genes and genomes. Nucleic Acids Res 28:27–30.

Kanehisa M, Goto S, Aoki-Kinoshita KF, Itoh M, Kawashima S, Katayama T, Araki M, Hirakawa M. 2006. From genomics to chemical genomics: New developments in KEGG. Nucleic Acids Res 34:354–357.

Kauffman KJ, Prakash P, Edwards JS. 2003. Advances in metabolic flux analysis. Curr Opin Biotechnol 14:491–496.

Kuyper M, Toirkens MJ, Diderich JA, Winkler AA, van Dijken JP, Pronk JT. 2005. Evolutionary engineering of mixed-sugar utilization by a xylose-fermenting Saccharomyces cerevisiae strain. FEMS Yeast Res 5:925–934.

Lawson JE, Gawaz M, Klingenberg M, Douglas MG. 1990. Structure-function studies of adenine nucleotide transport in mitochondria. I. Construction and genetic analysis of yeast mutants encoding the ADP/ATP carrier protein of mitochondria. J Biol Chem 265:14195–14201.

Lee S, Phalakornkule C, Domach MM, Grossmann IE. 2000. Recursive MILP model for finding all the alternate optima in LP models for metabolic networks. Comput Chem Eng 24:711–716.

Mahadevan R, Schilling CH. 2003. Effects of alternate optima on constraint-based genome-scale metabolic models. Metabolic Eng 5:264–276.

Mahadevan R, Edwards JS, Doyle FJ III. 2002. Dynamic flux balance analysis of diauxic growth in Escherichia coli. Biophys J 83:1331–1340.

Nielsen J, Villadsen J. 1994. Bioreaction engineering principles. New York, NY: Plenum Press.

Ostergaard S, Olsson L, Nielsen J. 2000. Metabolic engineering of Saccharomyces cerevisiae. Microbiol Mol Biol Rev 64:34–50.

Pharkya P, Burgard AP, Maranas CD. 2004. OptStrain: A computational framework for redesign of microbial production systems. Genome Res 14:2367–2376.

Reed JL, Famili I, Thiele I, Palsson BO. 2006. Towards multidimensional genome annotation. Nature Rev Genet 7:130–141.

Sainz J, Pizarro F, Perez-Correa FR, Agosin E. 2003. Modeling of yeast metabolism and process dynamics in batch fermentation. Biotechnol Bioeng 81:818–828.

Sauer U, Hatzimanikatis V, Hohmann HP, Manneberg M, van Loon AP, Bailey JE. 1996. Physiology and metabolic fluxes of wild-type and riboflavin-producing Bacillus subtilis. Appl Environ Microbiol 62:3687–3696.

Segre D, Vitkup D, Church GM. 2002. Analysis of optimality in natural and perturbed metabolic networks. Proc Natl Acad Sci USA 99:15112–15117.

Sonnleitner B, Kappeli O. 1986. Growth of Saccharomyces cerevisiae is controlled by its limited respiratory capacity: Formulation and verification of a hypothesis. Biotechnol Bioeng 28:927–937.

Steinmeyer DE, Shuler ML. 1989. Structured model for Saccharomyces cerevisiae. Chem Eng Sci 44:2017–2030.

Stephanopoulos GN, Aristidou AA, Nielsen J. 1998. Metabolic engineering: Principles and methodologies. New York: Academic Press.

Varma A, Palsson BO. 1994. Stoichiometric flux balance models quantitatively predict growth and metabolic by-product secretion in wild-type Escherichia coli. Appl Environ Microbiol 60:3724–3731.

Varner J, Ramkrishna D. 1999. Metabolic engineering from a cybernetic perspective. 1. Theoretical preliminaries. Biotechnol Prog 15:407–425.

Vaseghi S, Baumeister A, Rizzi M, Reuss M. 1999. In vivo dynamics of the pentose phosphate pathway in Saccharomyces cerevisiae. Metabolic Eng 1:128–140.

DOI 10.1002/bit